Ocean Dynamics
May 2021, Volume 71 Issue 5 Pages 601-612
https://doi.org/10.1007/s10236-021-01449-w
https://archimer.ifremer.fr/doc/00816/92795/

Eddy formation in the bays of Kamchatka and fluxes to the open ocean

L'Her Alexandre [1], Reinert Markus [1], Prants Sergey [2], Carton Xavier [1, *], Morvan Mathieu [1]

[1] LOPS/IUEM/UBO, Brest, France
[2] Pacific Oceanological Institute, Vladivostok, Russia

* Corresponding author : Xavier Carton, email address : xcarton@univ-brest.fr

Abstract :

The Eastern Kamchatka Current (EKC) is the western boundary current of the North Pacific subpolar gyre. Southeast of the Kamchatka Peninsula lies a large anticyclonic eddy, the Kamchatka Eddy (KE). This eddy is quasi-stationary. More generally, the oceanic region east of the EKC contains many eddies, several of them large and long lasting. Using surface currents derived from altimetry, particle tracking and a simple two-dimensional numerical model of fluid flow, we investigate the variability of this eddy field, the generation of eddies in the bays of Kamchatka by the EKC and fluxes of water to and from these bays. Firstly, we recover in our analysis of long-lasting eddies, the main eddies of the region. Among strong eddies, the parity bias favors anticyclones. Our numerical simulations give a possible explanation for the process of eddy creation in the bays of the peninsula and show that the northernmost bay produces most anticyclones. Then, we track forward the water particles from these bays and we determine their fate in the open ocean; southeastward and southwestward trajectories are the most frequent. We also track water particles backward from the KE site; they often drift near the Kamchatka coast, but others drift south of this site and remain there, a priori trapped in other eddies. This study confirms the complexity of mesoscale motions and water exchanges in this region.

Keywords : Kamchatka current, Kamchatka eddy, Sea surface height data, 2D numerical model, Flow instability, Vortex formation, Lagrangian analysis

1 Context and objectives

Kamchatka is a peninsula in the Northwest Pacific Ocean between 50^{o}N and 60^{o}N. It extends about 1000 km to the south and 500 km to the west from its northeastern connection to continental Asia. The shape of Kamchatka's eastern coastline south of the Bering Sea is dominated by three round bays in a row with along-shore diameters of 130 km to 200 km and cross-shore diameters of 50 km to 70 km. They are, listed from the north to south, the Kamchatsky, Kronotsky and Avachinsky bays, respectively identified as Ka, Kr and Av in figure 1. Offshore, the ocean bottom features a deep trench, the Kuril-Kamchatka trench, which runs from the Kamchatka Strait along the peninsula and the Kuril Islands, up to the north of Japan.

The Eastern Kamchatka Current (EKC) forms the western boundary current of the North Pacific Subpolar Gyre. It originates north of the Kamchatka Strait with water from the Bering Sea and flows south along the coast of Kamchatka. It then continues along the Kuril Islands, merges with water coming from the Okhotsk Sea and becomes the Oyashio. The EKC is mainly a surface current which exhibits seasonal variations (Solomon and Ahlnas, 1978; Khrapchenkov, 1991; Stabeno et al., 1994; Isoguchi et al., 1994; Isoguchi and Kawamura, 2002: it intensifies in winter, with speeds up to 30 cm/s, and weakens in summer, when it can sometimes be absent. Moving eddies of the EKC, generated in the Kamchatka bays, are then advected southwest (Solomon and Ahlnas, 1978; Stabeno et al., 1994; Zhabin et al., 2010).

The generation of mesoscale eddies was observed near the three main capes of Kamchatka (Solomon and Ahlnas, 1978; Stabeno et al., 1994; Zhabin et al., 2010; ISS Crew, 2012). There is also an evidence of the presence of a mesoscale quasi-stationary vortex feature near the southern tip of Kamchatka. The quasi-stationary "Kamchatka Eddy" (KE) was identified in the field of altimeter-derived sea level anomalies by Isoguchi and Kawamura (2003) and was observed by Rogachev et al. (2007). This KE is anticyclonic, surface intensified and has a radius at the surface in the range of 70 – 80 km. In the recent paper by Prants et al. (2020), a 25-year time series of altimetry-based Lagrangian maps of different indicators has been computed to conduct a continuous census of KEs starting from January 1, 1993 through December 31, 2018. In every year, a quasi-stationary KE was detected stagnating over the Kuril-Kamchatka trench for a long period of time, from a few months to a year. The typical eddy in this family, the KE2017, was sampled in September 2017 in a cruise to demonstrate a typical subarctic vertical structure of water masses in summer. Its entire life cycle has been investigated including formation in the Avachinsky Bay, strengthening, merger with another eddies, splitting, erosion and eventual decay.
The purpose of the present study is to investigate with simple means (satellite

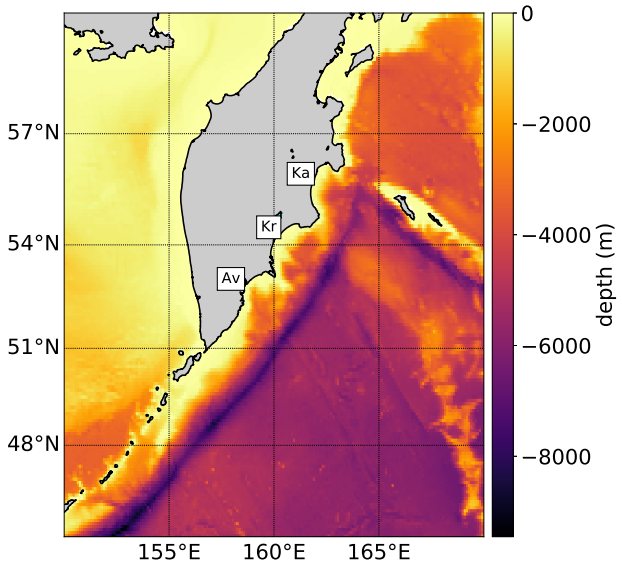

Figure 1: Bathymetry of the studied area, with names of the Bays. From North to South, Ka : Kamchatsky; Kr : Kronotsky; Av : Avachinsky. Source : GEBCO Compilation Group (2019) GEBCO 2019 Grid (doi:10.5285/836f016a-33be-6ddc-e053-6c86abc0788e)

data and a 2D numerical model) the eddies in this region, their generation in the bays, and their contribution to the KE. After presenting the model and the data (Section 2), we will successively study the variability and statistics of the eddies in the region (Section 3), the mechanism and conditions for eddy generation in a bay (Section 4), the origin of the KE, and its time evolution (Section 5). Of particular interest to this study are the questions: can the eastern coastline of Kamchatka play a role in the creation of the KE? If so, is a particular bay the origin of the KE water? What influences the KE south of the Kamchatka Peninsula?

2 Material and methods

2.1 Model

Considering the aspect ratio of the KE (1000 m in thickness for about 80 km in radius; e.g. the sampling of KE2017 reported by Prants et al., 2020), we consider that the fluid layer is thin with little vertical motion, except locally, so that the motion can be considered quasi two-dimensional (horizontally). The temporal evolution of such a system is determined by the condition that the

quasi-geostrophic potential vorticity q is conserved following the fluid motion:

$$dq/dt = 0, \quad d/dt = \partial_t + u\partial_x + v\partial_y$$

The potential vorticity is given by

$$q = \nabla^2\psi - \frac{\psi}{R_d^2} + f_0\frac{H_B(x,y)}{H} + f\,,$$

where ψ is the streamfunction of the flow; R_d is the deformation radius; f_0 is the local Coriolis parameter and $f = f_0 + \beta y$ its meridionally varying form; H is the total thickness of the flow and H_B is the height of topography.

For the Kamchatka situation, f_0 is about 10 radians per day and β approximately 10^{-3} rad/km/d. The external deformation radius varies between 1420 km and 2320 km, the internal deformation radius has values between 10 km and 20 km.

We use two configurations of the model:

1. a meridionally periodic channel on the f-plane, in which a meridional current is forced along the coast by a constant-in-time vorticity-forcing of the form $2\tau x/\sigma^2 \exp(-x^2/\sigma^2)$; the model is initialized with a white noise in vorticity of weak amplitude over the whole domain to destabilize the alongshore jet; the objective of this configuration is to study the stability of this jet along the coast and the influence of bays; this is the local approach;

2. a closed domain on the β-plane, in which a double gyre circulation is forced by the zonal wind stress:

$$\tau_x = -\tau_0 L_y/(2\pi)\cos(2\pi y/L_y)\,.$$

   In this case, the current is steady on the beta-plane. Again we investigate the influence of coastal irregularity. This is the global approach.

Numerically, the finite-difference model (Roullet, 2017) solves the vorticity equation spatially with a fifth order interpolation on 256×256 grid points with upwind fluxes and no explicit diffusion. For the time-stepping scheme, a strong stability preserving third-order Runge Kutta method is used.

2.2 Data

The dataset used in our study is the Global $1/4^o$ AVISO Altimetry product. We focused on the area between 150^oE, 45^oN and 170^oE, 60^oN containing the Kamchatka Peninsula and the main eddies of interest. For the statistical studies, we used the historical 26 years dataset at one frame per week. This provided

enough data to derive statistically relevant quantities. For Lagrangian studies we used a recent time series of 555 days at a daily frequency. Indeed, when integrating the positions of particles using the velocity field, having only one data per week leads to large errors and to jumps in the trajectories. That is why daily data were used then.
The data in the region were first analysed with Empirical Orthogonal Functions (EOF) using the python library "eofs" (Dawson, 2016). The technique of EOF decomposes a spatio-temporal field into a set of orthogonal patterns in space and uncorrelated time series corresponding to the patterns (Hannachi et al., 2007). We used EOFs to obtain the patterns and variations of sea surface height (SSH). Eddy tracking was done using AMEDA (Angular Momentum Eddy Detection and tracking Algorithm; LeVu et al., 2018); AMEDA uses the local normalized angular momentum (LNAM) and the detection of closed streamlines to track the eddies. The LNAM has an extremum at the center of an eddy, which has a value of 1 for a cyclonic eddy and -1 for an anticyclonic one. LNAM is used to detect the center of the eddy, together with the local Okubo-Weiss parameter, defined as:

$$OW = Sn^2 + Sh^2 - \omega^2$$

where Sn is the normal component of strain, Sh is the shear component of strain and ω is the relative vorticity. This parameter indicates if the flow is dominated by deformation (if $OW > 0$) or by vorticity ($OW < 0$).
The local OW parameter was used to confirm that the detected eddy center is in a vorticity-dominated region of the flow. Then, to ensure that the LNAM extremum is indeed an eddy center, the algorithm keeps the extremum only if there exists closed streamlines around it.

In AMEDA, eddy tracking is performed using a cost function that minimizes the difference in SSH between two successive detections of an eddy, in a given search area, subject to a maximal drift speed of the eddies (set to 6.5km/day by default). This algorithm also handles interactions between eddies such as splitting and merging by detecting streamlines that enclose two eddy centers (called characteristic shared contour). If the mean velocity in this shared contour is higher than the maximum velocity of at least one of both eddies, an interaction is detected. Once this occurs, AMEDA detects if there has been a splitting or a merging of the eddy by computing the number of trajectories before and after the interaction. Here, we used the recommended settings of AMEDA, given in the Le Vu et al., 2018 work.

From SSH, we also computed the trajectories of numerical particles. The positions were integrated from the geostrophically derived velocity fields using a 4th order Runge-Kutta scheme. The timestep was set to 0.2 days to avoid blowups. The velocity fields were interpolated at each step using optimal interpolation in

space, and linear interpolation in time.

3 Eddy variability near the Kamchatka Peninsula

3.1 Eddy variability

Here we present results from our analyses of the long term variability of relevant quantities, such as Sea Level Anomaly (SLA). These analyses where done over the 26 year data, one data frame per week. We used the method of EOFs to find orthogonal patterns and their periodicity. We plot only the first 6 EOF modes, because further modes have a really low contribution to the total variance of the fields.

The variability of the Sea Level Anomaly (SLA) around Kamchatka is characterized, in its first mode, by a clear regional oscillation with a period of 1 year, with a minimum in winter and a maximum in summer (see Figure 2). This mode has been discussed in the literature and corresponds to the steric variation of the sea level (Isoguchi et al., 1997). It clearly presents an increasing trend that can be related to global warming (Vermeer and Rahmstorf, 2009; Yeo and Kim, 2014). The second subplot of Figure 2a shows the second EOF mode; it is related to the KE in position and recurrence. It has a main periodicity of 25 years, found by calculating the periodogram of the principal component (not shown here). But this result has to be taken *cum grano salis* as we only have 26 years of data. This period is close to that of the Pacific Decadal Oscillation (PDO) or the North Pacific Gyre Oscillation (NPGO) (Chhak et al., 2009). Following the results of Chhak et al. (2009), the NPGO has a maximum between the year 2000 and 2005, which corresponds to the maximum of the second mode. This mode also has a minimum every year around the months of December and January, corresponding to the winter intensification of the EKC. Its maximum is around the middle of the year, in relation to the observations of the KE in summer. Given the position of the maximum of this EOF mode and its variability, it identifies the KE.
The third mode has a yearly period and also presents an oscillation over 25 years as the second mode, but out of phase. The second and third modes can be related: indeed the presence of the KE is related to a SLA oscillation between the north and the south of the Aleutian Islands. The three last modes describe the presence of the KE in relation with neighboring eddies, in particular the Aleutian eddies. Thus, these eddies are coherent structures in our 26 years of data (see also Prants et al., 2020). Both fourth and fifth modes have a frequency of 0.6 cycles/years (approximately a period of 1.7 years) which is not explained here. The sixth mode has 1 and 5 year periods. The yearly periodicity is related to seasonal variations between hot and cold months. The 5 year periodicity can be

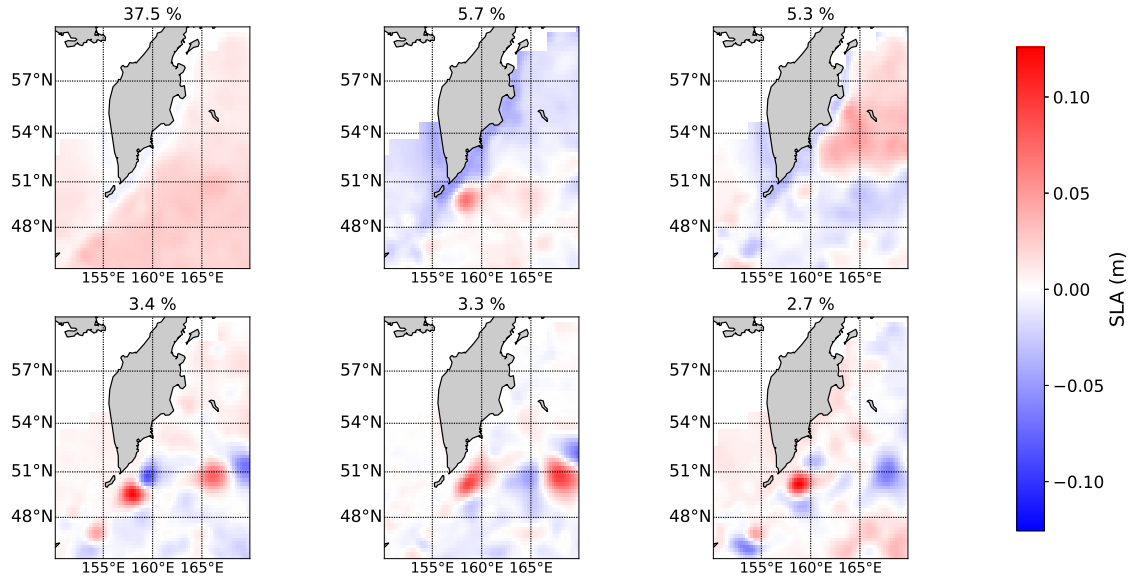

(a)

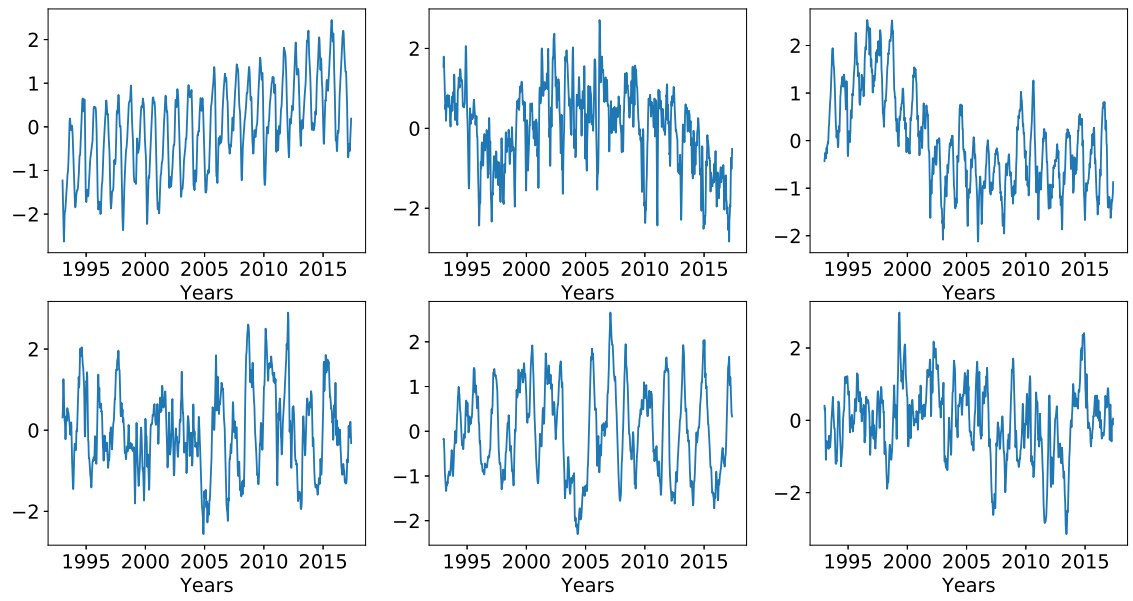

(b)

Figure 2: Sea level anomalies Empirical Orthogonal Functions (a); sea-level anomalies principal component time series (b)

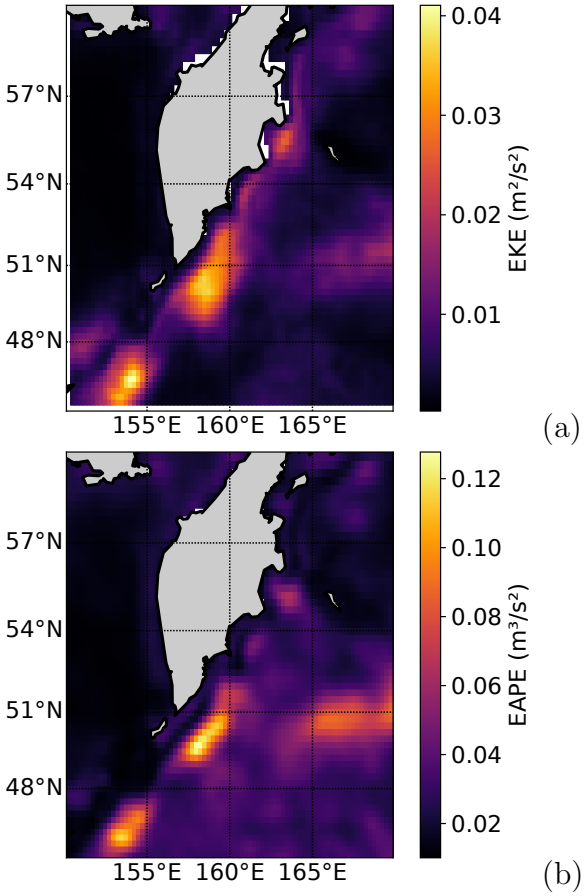

Figure 3: Maps showing the distribution of (a) surface EKE; (b) surface EAPE, computed from altimetry

related to ENSO, which has a periodicity between 2 and 7 years (Yeo and Kim, 2012; Lu et al., 2018). In particular, the sixth principal component has minima in 1998, 2007, 2011–2012, 2014 and a maximum in 2015 which correspond to those of the NCEP-NCAR Reanalysis Multivariate ENSO index.

3.2 Eddy statistics

The eddy kinetic energy (EKE) and the eddy available potential energy (EAPE) (defined as $g\eta^2/2$ where η is the SLA), averaged over 26 years of data clearly show the presence of the KE (see Figure 3).

The EKE maximum South of Kamchatka corresponds to the area where the KE is observed. The strong EKE south of 48^oN and west of 155^oE corresponds to the north of the Oyashio Current. EKE is also strong near the 3 capes of the

Kamchatka Peninsula, in particular in the Kamchatsky Bay, corresponding to the presence of eddies in this region. A slightly weaker spot of EKE, around 51^oN and east of 165^oE, is associated to an eddy generated south of the Aleutian Islands, in the western Alaskan Stream region between 175 and 170^oE. Indeed, these Aleutian eddies, formed just over the Aleutian Trench, can stagnate in this region for a while. After detaching from the Alaskan Stream, they move by the planetary beta effect via a regular southern route to Kamchatka and then decay before reaching the Kamchatka trench.
Such EKE signatures in the 26 year mean shows that those features are recurrent (see also Prants et al., 2020). The regions of high EAPE concentration correspond to those of EKE. North of the Oyashio, south of Kamchatka and of its capes, high energy concentration is due to the frequent presence of intense eddies. High values of EKE and EAPE in the area $45 - 48^o$N are explained by the regular presence of the Bussol anticyclonic eddy (Yasuda et al., 2000, Prants et al 2016, Prants et al 2017). The EKE and EAPE values in the area $164 - 170^o$E reflect the regular route of migration of Aleutian eddies from the Alaskan Stream.
We used AMEDA to track the eddies over 2 years starting from January, 4 1993, the first day of available altimetric data. We split the data into two series for practical convenience: from 1993-01-04 to 1995-01-02 and from 1995-01-02 to 1997-01-06. In total, 1430 eddies were detected during the first period, 49.7% of them cyclonic and 50.3% anticyclonic. During the second period, 1420 eddies were detected, 49.9% cyclonic, 50.1% anticyclonic. Having detected the eddies, we also obtained statistics of their characteristics, such as their vorticity, their size, or their lifetime (Figure 4). In these histograms the eddies are counted once for every date they were detected, except for that of lifetime. The statistical distributions are similar for the two series. The vorticity histograms show that more anticyclones have high magnitudes compared to the cyclones. This can be related to the in situ observations of eddies, mentioned above.
As already observed in other parts of the ocean (Liu et al., 2012), we find an exponential decay in the number of eddies with respect to their lifetime. This decay can be related to the interactions of eddies among them, with regional currents, or with topography. The dispersion of eddies into Rossby waves during their westward propagation, and the peripheral mixing of the eddy core water with surrounding waters, are two other mechanisms leading to eddy decay. Finally, the ventilation of warm surface eddies can also lead to their attenuation. Which mechanism prevails here should be assessed with an eddy-resolving, primitive equation model, which is beyond the scope of this paper.

4 Eddy generation and evolution in a bay

In this section, we present the results obtained with our numerical model, using an idealized configuration of the Kamchatka Peninsula and the EKC to explain

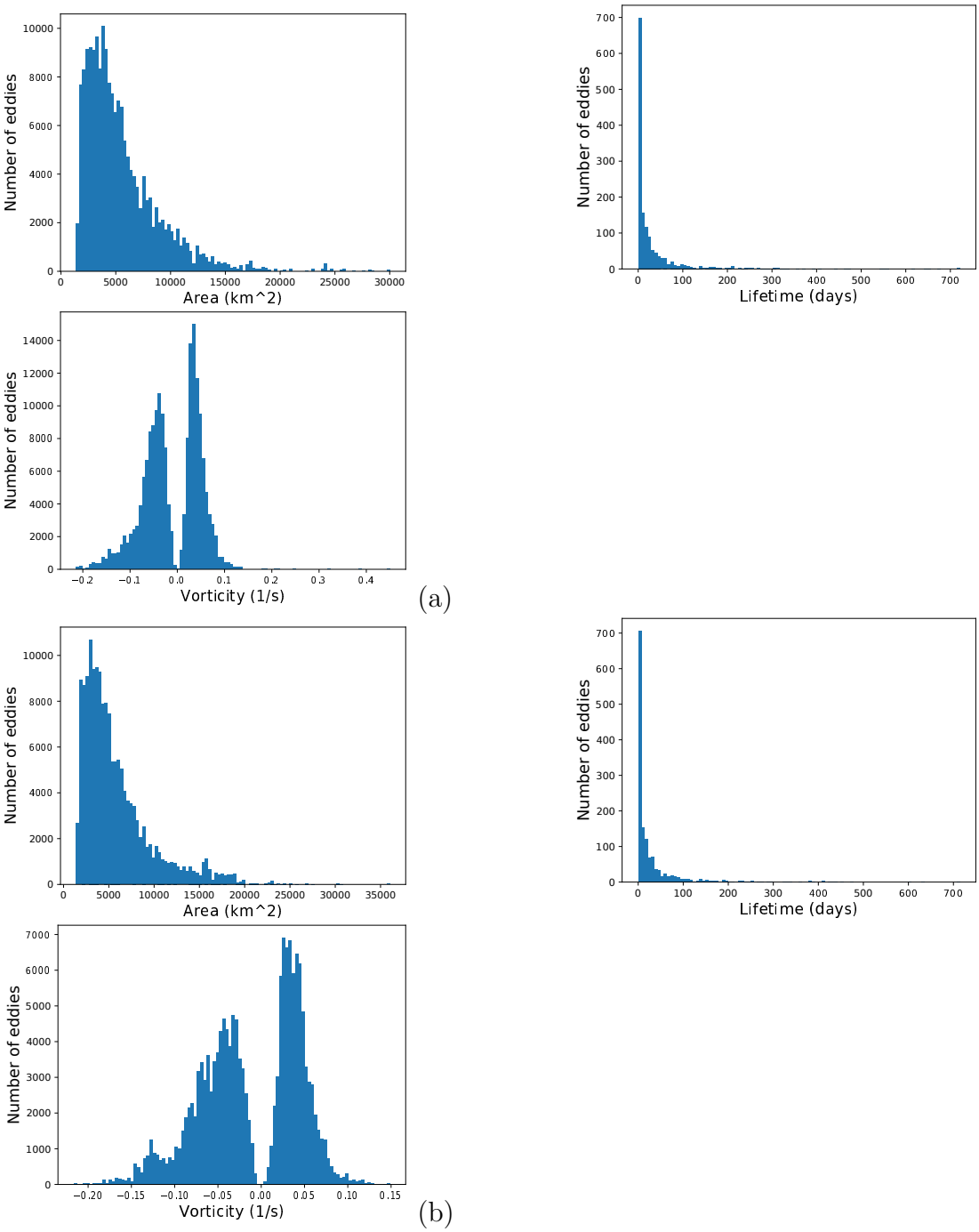

Figure 4: Characteristics of eddies (area, lifetime, number of eddies) in the Kamchatka region for (a) the first time-series; b) the second time-series

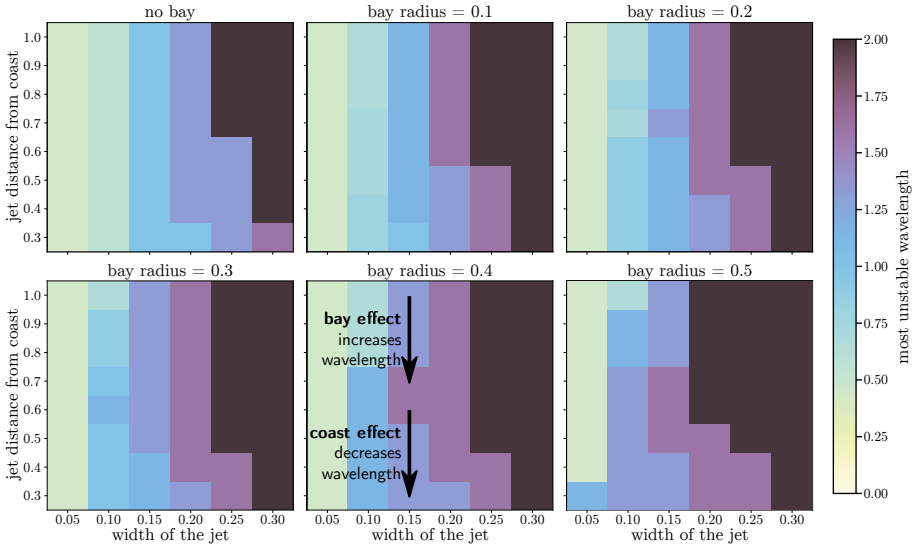

Figure 5: Most unstable wavelength for a straight current along a coast with a bay.

the formation of eddies in a bay by a coastal current. These simulations will help determine the origin of the KE.

4.1 Vortex formation by a jet along a straight coast

As a preliminary analysis, we investigated the instability of a current along a straight coast on the f-plane in a 2D model with flat bottom and infinite deformation radius ($R_d^{-1} = 0$). Changing the distance between the coast and the current modifies two properties of the shear instability of the jet:
Firstly, meanders cannot extend shoreward more than the distance to the coast. Thus, if eddies are generated by meander occlusion, they will be closer to each other and to the coast. Therefore, the joint propagation of two opposite sign vortices is the dominant process for an unstable current close to the coast, while vortex merging is the prevailing process in a current far from the coast.
Secondly, the wavelength of the most unstable mode is smaller if the current is close to the coast. This can be seen in the top left panel of Figure 5, which shows the most unstable wavelength for jets of different widths and varying the distance to the coast. Thus, for narrow jets, which naturally develop short meanders, the most unstable wavelength is not visibly altered by the distance between the current and the coast. On the contrary, wider jets, which naturally have longer wave instabilities, become unstable to shorter perturbations when their distance to the coast is reduced.

4.2 Vortex formation by a jet along a coast with a bay

This is not always true if the coast is indented by a semi-circular bay. In this case, we observe two distinct effects influencing the wavelength of the most unstable mode in the shear instability.

On the one hand, the most unstable wavelength on the jet increases with increasing bay-size, that is, from one frame in Figure 5 to the next. This "bay effect" is stronger, the wider the current is and the closer it is to the coast; so for a narrow jet, the presence of the bay plays a role only if the flow is near the coast.

On the other hand, the wavelength decreases when the distance between jet and coast decreases, that is, towards the bottom of every frame in Figure 5. This is the "coast effect" that we have already observed for a completely straight coast in the previous section.

Our simulations show that the bay effect dominates for narrow jets, while the coast effect dominates for wider jets. In between these extreme cases, the two opposing effects act against each other. This means, as a medium-sized jet approaches a coast with a bay, the wavelength of the most unstable mode increases at first, but decreases afterwards (see the arrows in Figure 5).

In conclusion, a coastal current interacts with the straight part of the coast as well as with the coastal embayment. The interaction with the straight coast reduces the length of the meanders, while the bay creates the opposite effect. Depending on the width of the jet, the size of the bay, and the distance between flow and coast, one effect or the other dominates.

The time evolution of vorticity maps from this model, presented in Figure 6, brings another element of explanation for the Kamchatka situation. Here, the jet has a piecewise-linear velocity profile instead of a Gaussian shaped one, since the vortices in the linear case have sharper boundaries, and thus the result is clearer. In this situation, the vortices created close to the bay can be "trapped" between the capes. These trapped vortices have a core of negative vorticity and remain quasi steadily in the bay, while acquiring additional vorticity from neighboring turbulence. Thus they grow and survive longer than vortices which are not near the capes. A necessary condition for this growth of vortices in bay is that the southward jet be close to the coast and thereby stabilizes the vortices against the mirror vortex effect which pushes them northward. At some point in time, however, this balance breaks and these vortices leave the bay. What happens then is not studied with this model; particle tracking with the geostrophic surface flow (from altimetry) will provide information (see the following section); vortex pathways are discussed in the final section of this article.

These model results are confirmed by a careful inspection of altimetry-based daily Lagrangian drift and Lyapunov maps of the KE2017 sampled in a cruise by Prants et al., 2020. This eddy was born in the beginning of April 2017 as a result of meandering of the EKC in the Avachinsky Bay with the initial size of about 60×80 km. After formation, it was trapped in the Bay for a while and then

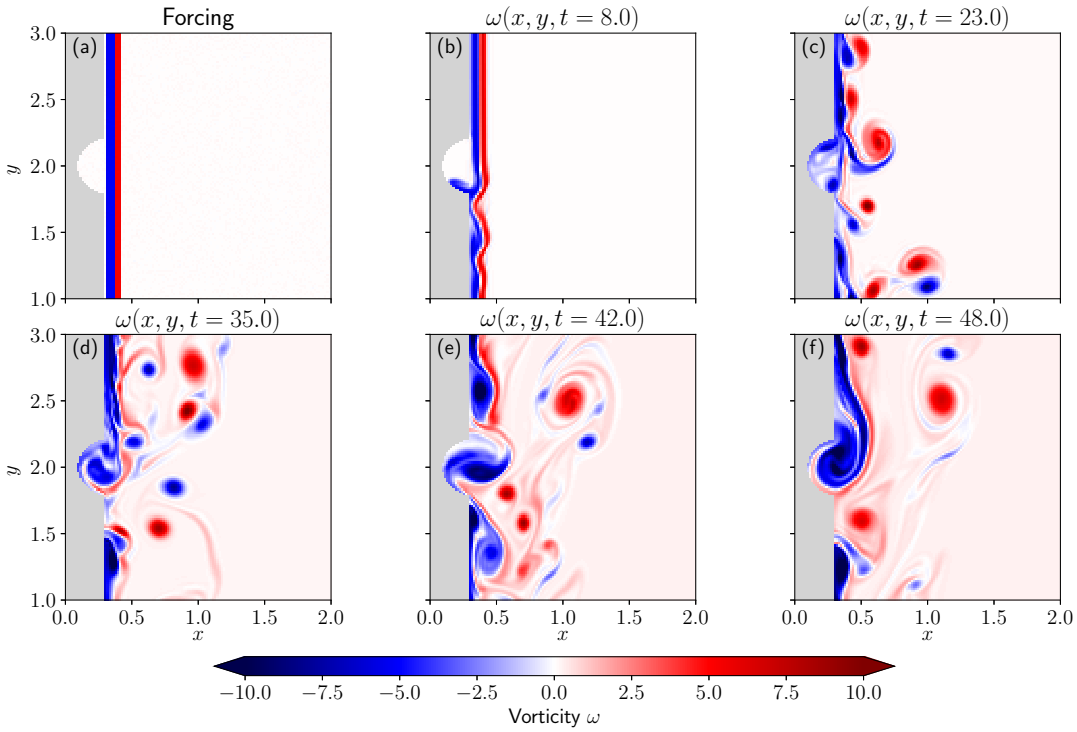

Figure 6: Time evolution of the relative vorticity of an unstable current along a coast with a bay. The anticyclonic (cyclonic) vorticity is in blue (red).

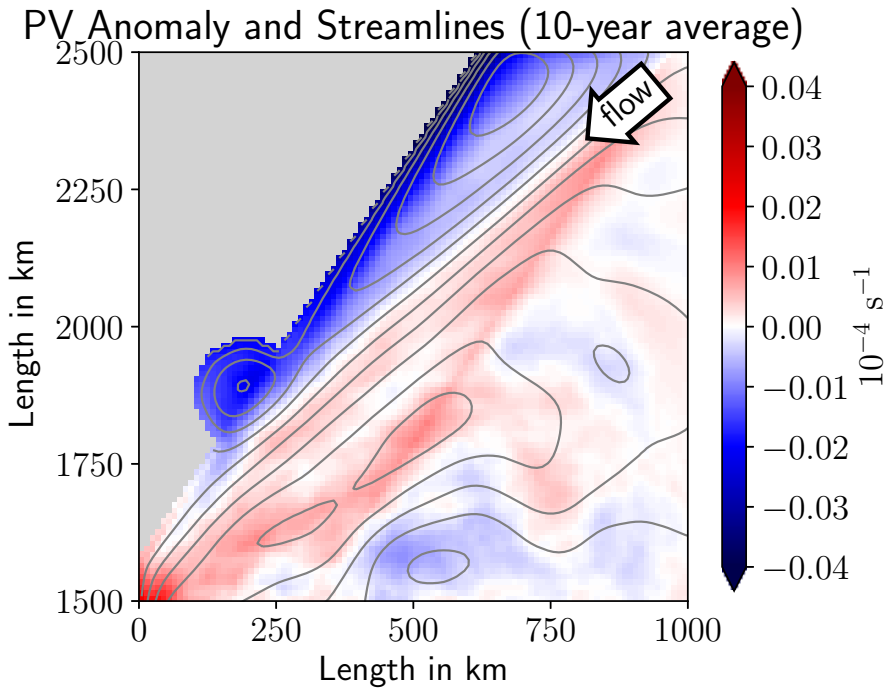

Figure 7: Potential vorticity anomaly and streamlines in the northwestern part of the double gyre simulation.

left it being advected by the EKC southward increasing gradually in size due to a merger with another anticyclonic eddies. After reaching the western slope of the Kuril-Kamchatka trench in the beginning of May 2017, it stagnated over the trench during almost 8 months, then split and dispersed eventually.

4.3 Vortex formation in a bay by a double gyre flow

Finally, we use the more complete model: a double gyre forced by the wind, with beta-effect, finite deformation radius, and bottom topography. We consider here that the deformation radius is the external one; another simulation with an internal radius of deformation (not shown) did not yield significant differences with the results presented here.

Here we modeled the bottom topography with three components: a continental shelf at the coast, followed offshore by a linear slope, and then the flat abyssal plain. The slope must not be too steep to stay consistent with the assumptions of the quasi-geostrophic model. Nevertheless, this is not a harsh limitation, since even a small continental shelf makes that the western boundary current develops mainly along the continental slope, at some distance from the coast (see the arrow

in Figure 7).
Also, in the southern half of the domain, a western boundary current develops, flowing northward. Where the two currents meet, turbulence grows. This turbulence is shielded away from the coastal area by the continental slope. Therefore, the dynamics at the coast is not dominated by turbulent effects but it is rather determined by the southward flowing current.
If the coastline features a bay, then a part of the southward flowing western boundary current enters this bay and recirculates there. It creates an anticyclone in the bay, which aggregates vorticity over time. This is shown in Figure 7, which presents the anomaly of potential vorticity and the streamlines in this simulation, averaged over 10 years. The southwestward flow with an average velocity of about 6 cm/s goes partly into the bay and curves along the circular boundary of the bay; via flow curvature, it creates a patch of negative vorticity which grows as an eddy.
This eddy might leave the bay when the incoming current diminishes, as observed for the EKC in summer. However, this has not yet been observed with this numerical model and this will be further investigated by tracking floats.

5 Origin and evolution of the Kamchatka eddy

5.1 Lagrangian particle trajectories

To obtain a wider and more complete view of the evolution of the eddies created in the three bays and of their further evolution towards the KE, Lagrangian particles were seeded in the surface flow field obtained by geostrophic balance from sea surface height. The particle positions were integrated backward as well as forward in the velocity field to determine the origin and destination of the water masses in the KE.

5.1.1 Backward integration

Figure 8a shows the 166 day backward integration of particles seeded in spring 2018. By this time, the KE2018 was located to the east off the trench, outside the blue seeded areas shown in Figure 8a (see Table 1 and Fig. 13 in Prants et al., 2020). We used the same initial velocity field for all plots in this figure so they can be compared. Most particles come from the coast of Kamchatka. This confirms that eddies coming from the capes, created by the interaction of current with the coast, are advected towards the KE.
When particles are seeded north of 48^oN, most of them travel over large distances from the Kamchatka coast, or even coming from farther north. When particles are seeded south of 48^oN, some of them come from the Kamchatka coast but most of them stay in the area, south of 51^oN. Thus, the along-shore flow becomes

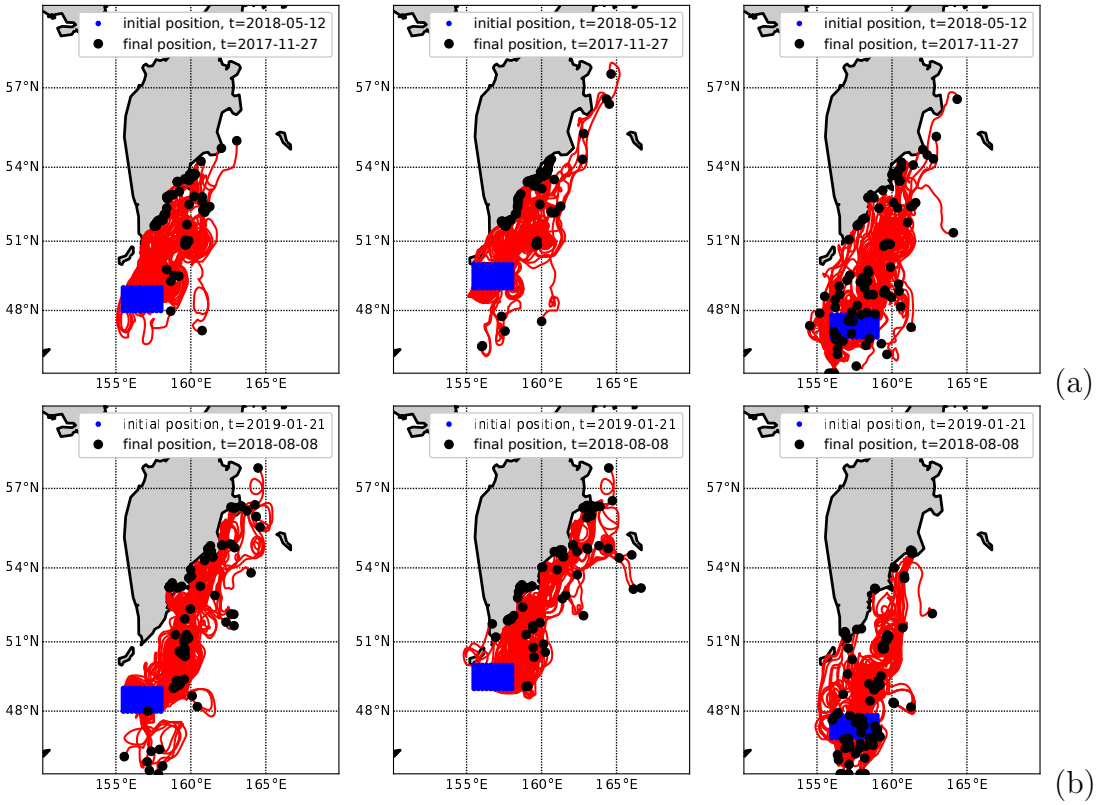

Figure 8: Trajectories of particles seeded in the KE, or north of the KE or south of it (a) in spring 2018; (b) in winter 2019.

irregular south of 48^oN, with many eddies trapping the seeded particles for a long time. Those eddies likely correspond to the Bussol eddies, which have been observed in the area around $45^o - 48^o$N (Yasuda et al., 2000, Prants et al 2016).

In Figure 8b, particles are seeded at the same place as in Figure 7a, but now in winter 2019, when the KE was present in the area. Note that the KE may remain in this area in different seasons (see Table 1 in Prants et al., 2020).
It appears that more particles come from the south in winter. But a careful examination of daily velocity and Lagrangian maps over the 1993-2019 period did not show events when eddies from the south contributed to maintain the KE at its place. After stagnating over the trench, the KE migrates to the south where it can trap particles seeded south of 48N.
Therefore, when the KE remains stationary, another mechanism like interaction with topography or with atmospheric forcing should be assessed.

5.1.2 Forward integration

To determine definitely that some of the water in the KE comes from the capes, we seeded particles in each of the 3 capes and integrated the velocity field forwards. We show the results in Figure 9. Here again we used the velocity fields derived from ADT to have the full dynamics of the ocean. The particles were integrated forward for 200 days.

Figure 9A shows the 200-day forward integration of particles seeded in fall 2017, (when the KE was present) until the beginning of the following summer. Figure 9B shows the results of forward integration of particles seeded in spring.
In Figure 9A, most of the particles seeded in the bays go southwest, along the Kamchatka Peninsula. On their way, they travel to the KE, located around 50^oN, 158^oE, and then may exit it from the south and southwest. A few particles move southeastward, between the KE and the Aleutian eddy; this particle motion is rather due to the configuration of the eddies there. Such a motion was previously noticed for surface buoys (Stabeno et al., 1994).
As can be seen from Figure 8a, the flow from the Kamchatsky Bay is coherent: all the trajectories are parallel; they start to diverge as they move past Kronotsky Bay. The particles exiting from Kronotsky Bay have close trajectories at the beginning, but they rapidly enter an eddy and their trajectories become irregular. Finally, the particles from the Avachinsky Bay have chaotic trajectories right from the beginning.
These observations support our picture of the flow characteristics: as seen in Figures 8a and 8b, the flow south of Kamchatka is more turbulent than the flow along the coast, though this latter has an intense branch interacting with the coast. Reminding Figure 2a showing the eddy kinetic energy averaged over 26 years: along the coast, the EKE mainly intensifies at Avachinsky Bay. The La-

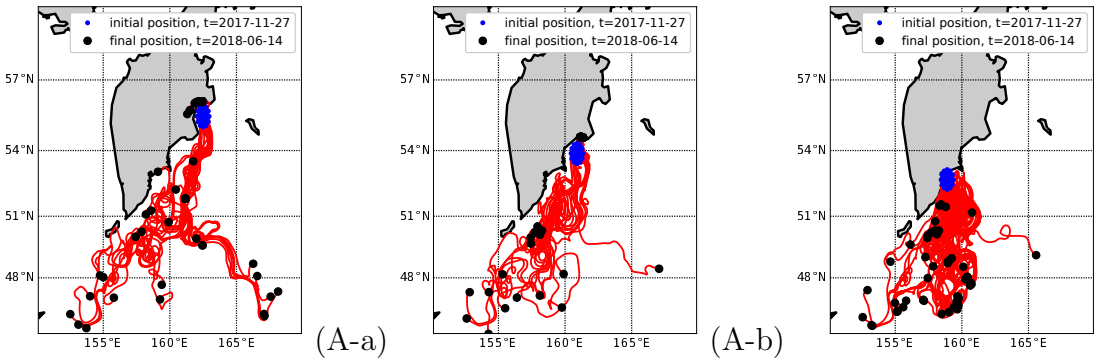

Figure 9: Trajectories of particles seeded at the capes, (A) during the fall 2017; (B) in spring.

grangian analyses support this conclusion: the flow becomes turbulent mainly south of Avachinsky Bay.

In Figure 9B, a few trajectories are different from those in Figure 8a. In particular, in Figure 9B-a, the particles seeded at Kamchatsky Bay do not drift as far as the same particles seeded in fall: they remain trapped in eddies. This occurs in particular in the KE at its location at that time, around 160^oE, 50.7^oN. This is another hint that water from the capes gets trapped in the KE.
The other plots of Figure 9 do not show substantial differences in trajectories between fall and spring. The particles are advected southwestward and get trapped in eddies present in the area, in particular the KE. The particles from Kronotsky and Avachinsky Bays escape the eddies and travel southeastward and southwestward as observed previously. Note that the particles originating from Kamchatsky Bay do not escape the KE, while others do. Further work will study how long the particles coming from the different capes stay trapped in the KE.

The velocity of the seeded particles was calculated, along with the mean and the maximum; the results are shown in tables 1 and 2.

Origin	Cape 1	Cape 2	Cape 3
Fall	5 cm/s	4 cm/s	10 cm/s
Spring	7 cm/s	7 cm/s	9 cm/s

Table 1: Mean velocity of the particles over the 200 days of integration

Origin	Cape 1	Cape 2	Cape 3
Fall	58 cm/s	57 cm/s	62 cm/s
Spring	57 cm/s	65 cm/s	61 cm/s

Table 2: Maximum velocity of the particles over the 200 days of integration

Results are comparable with those found by Stabeno et al. (1994). Indeed, for the EKC, they found mean velocities of drifters from 2 to 50 cm/s and daily maximum velocities ranging from 13 to 86 cm/s, depending on the buoy. The differences in mean velocities between our analysis and the drifting buoys is likely due to the wind-drag effect and the resolution of our velocity fields.

6 Summary and discussion

This study of currents and eddies east of the Kamchatka Peninsula revealed the main modes of variability in this area, which can be correlated to observed variations of the Pacific Ocean such as ENSO or PDO. The eddy energy near Kamchatka also clearly shows the KE, the Aleutian eddies, and the variability along the coast of Kamchatka.

The diagnostics calculated from AMEDA show that Kamchatsky Bay is a region of strong kinetic energy for anticyclonic eddies, and a site of strong enstrophy accumulation. Kamchatsky Bay is an important contributor of eddies. Avachinsky Bay also sheds eddies which merge with the KE.

6.1 Results of the modeling study

A simple numerical model was used to show that a meridional jet as well as a western boundary current can generate eddies near a coast and in particular in a bay. Thus we answered positively our first question: Indeed, the eastern coastline of Kamchatka with its bays plays an important role for the creation of the KE. Using altimetric data, we showed that, in particular, Kamchatsky Bay sheds more eddies which then merge with the KE.
Since the modeling study used a highly idealized situation, it did not answer the question of how anticyclones forming in the bays propagate southward to the site of the KE. Several processes can be able to explain this southward drift. First of all, the vortices can be advected by the EKC. Secondly, the planetary β-effect is known to lead to a southwestward drift of anticyclonic eddies. We did not observe eddy shedding from the bay in our simulations perhaps because the flow was not intermittent enough to release the eddies formed in the bay. Another possibility for southward advection of eddies is via topographic Rossby waves on the continental slope. Finally, friction in the coastal boundary layer can generate small eddies which influence the evolution of the larger anticyclones while they are still in the bay. A further study with a 3D model will concentrate on these effects.

6.2 Results of the Lagrangian study

Even without direct proof from our idealized model, particles seeded in the regional flow (computed geostrophically from altimetric data) indicate that the eddies formed in the bays of the Kamchatka Peninsula undergo a southwestward drift. These results are consistent with the results by Prants et al., 2020 who tracked the drift of bay eddies using altimetry-derived Lagrangian maps. Therefore, the KE is fed by water coming from these bays. The trajectories showed that the journey from the bays to the KE takes about 5 to 6 months and is marked by a seasonal variability. We also showed that water from the Okhotsk sea wraps around the KE and may enter it. Thus we determined preferential origins for water in the KE.
The forward and backward trajectories of the seeded particles show that water coming from the bays and capes is advected southwestward at a speed depending on the EKC. These results are similar to those by Stabeno et al. (1994), who tracked drifters in the EKS. They found that most drifters go southwestward after

passing through eddies and that some drifters may go southeastward between the Aleutian eddy and the Kuril-Kamchatka eddies.
Further analyses should be carried out in a regional, primitive-equation model, to better assess the interactions and decay mechanisms of eddies in this region. Another point of interest which should be addressed in such models are the mechanisms which contribute to the stationarity or to the motion of the KE. This will be the subject of further studies.

Acknowledgements
This work was achieved in partial fulfilment of A. L'Her and M. Reinert, students for an MSc degree in Physical Oceanography at UBO. The MSc studies of M. Reinert are supported by the MOPGA grant of the French government. The work of SP was supported by the Russian Science Foundation (project no. 19-17-00006).

7 References

Chhak K.C., Di Lorenzo E. Schneider N. and P.F. Cummins, 2009: Forcing of low-frequency ocean variability in the Northeast Pacific. J. Clim., 22, 5, 1255-1276.
Dawson, A., 2016. eofs: A Library for EOF Analysis of Meteorological, Oceanographic, and Climate Data. J. Open Res. Soft., 4, 1, e14. DOI: http://doi.org/10.5334/jors.122
Hannachi A., Jolliffe I.T., and D. B. Stephenson, 2007: Empirical orthogonal functions and related techniques in atmospheric science: A review. Int. J. Clim., 27, 9, 1119-1152.
Isoguchi O., Kawamura H., and T. Kono, 1997: A study on wind-driven circulation in the Subarctic North Pacific using Topex/Poseidon altimeter data. J. Geophys. Res. Oceans, 102, C6, 12457-12468.
Isoguchi, O., and H. Kawamura, 2002: Wind-driven circulation in the Subarctic North Pacific using altimeter data. J. Earth Syst. Sci., 111, 3, 267-279, doi:10.1007/BF02701973.
Isoguchi, O., and H. Kawamura, 2003: Eddies advected by time-dependent Sverdrup circulation in the Western Boundary of the Subarctic North Pacific. Geophys. Res. Lett., 30, 15, 1-4, doi:10.1029/2003gl017652.
ISS Crew, 2012: Photo of ice floes along the Kamchatka coastline. NASA Earth Observatory, URL https://earthobservatory.nasa.gov/ images/77589/ice-floes-along-the-kamchatka-coastline.
Khrapchenkov, F.F., 1991: Peculiarities of hydrological structure in Avachinsky Bay in winter 1989. Okeanologiya, 31, 6, 949-954. [in Russian].
Le Vu B., Stegner A., and T. Arsouze, 2018: Angular momentum eddy detection and tracking algorithm (ameda) and its application to coastal eddy formation. J. Atmos. Ocean. Tech., 35, 4, 739-762.

Liu Y., Dong C., Guan Y., Chen D., McWilliams J.C., and F. Nencioli, 2012: Eddy analysis in the subtropical zonal band of the North Pacific Ocean. Deep Sea Res. Part I: Oceanogr. Res. Papers, 68, 54-67.
Lu B., Jin F.F. and H.L. Ren, 2018: A coupled dynamic index for ENSO periodicity. J. Clim., 31, 6, 2361-2376.
Prants S.V., Budyansky M.V., Lobanov V.B., Sergeev A.F. and M.Yu. Uleysky, 2020: Observation and Lagrangian analysis of quasi-stationary Kamchatka trench eddies. J. Geophys. Res. (Oceans), 125, 6, e2020JC016187, https://doi.org/10.1029/2020JC016187.
Prants S.V., Lobanov V.B., Budyansky M.V., and M. Y. Uleysky, 2016: Lagrangian analysis of formation, structure, evolution and splitting of anticyclonic Kuril eddies. Deep-Sea Res. Part I-Oceanogr. Res. Papers, 109, 61-75.
Prants S.V., Uleysky M. Yu. and M.V. Budyansky, 2017: Lagrangian oceanography: large-scale transport and mixing in the ocean. Springer Verlag. Berlin, New York. 271 p.
Rogachev K., Shlyk N. and E. Carmac, 2007: The shedding of mesoscale anticyclonic eddies from the Alaskan stream and westward transport of warm water. Deep-Sea Res. Part I-Topical Studies in Oceanography, 54, 23-26, 2643-2656.
Roullet, G., 2017: Fluid2d documentation. URL https://pagesperso. univ-brest.fr/roullet/fluid2d.
Solomon, H. and K. Ahlnas, 1978: Eddies in the Kamchatka Current. Deep Sea Res., 25, 403, doi:10.1016/0146-6291(78)90566-0.
Stabeno, P.J., Reed R.K. and J. Overland, 1994: Lagrangian measure- ments in the Kamchatka Current and Oyashio. J. Oceanogr., 50, 653-662, doi:10.1007/BF02270498.
Stommel, H., 1948: The westward intensification of wind-driven ocean currents. Eos, Transactions American Geophysical Union, 29, 2, 202-206, doi:10.1029/TR029i002p00202.
Vermeer M. and S. Rahmstorf, 2009. Global sea level linked to global temperature. Proc. Nat.l Acad. Sci., 106, 51, 21527-21532.
Yasuda, I., and Coauthors, 2000. Cold-core anticyclonic eddies south of the Bussol Strait in the Northwestern Subarctic Pacific. J. Phys. Oceanogr., 30, 6, 1137-1157.
Yeo S.R. and K.Y. Kim, 2014. Global warming, low-frequency variability, and biennial oscillation: an attempt to understand the physical mechanisms driving major ENSO events. Clim. dyn., 43, 3-4, 771-786.
Zhabin I.A., Lobanov V.B., Watanabe S., Wakita M., and S.N. Taranova, 2010. Water exchange between the Bering Sea and the Pacific Ocean through the Kamchatka Strait. Russian Meteorology and Hydrology, 35, 3, 218-224.

GEBCO Compilation Group (2019) GEBCO 2019 Grid (doi:10.5285/836f016a-33be-6ddc-e053-6c86abc0788e)